Stability and pull-in voltage of electrostatic parallel-plate actuators in liquid solutions

Anne-Sophie Rollier, Bernard Legrand, Dominique Collard, Lionel Buchaillot

The stability and pull-in voltage of electrostatic parallel-plate actuators in liquid solutions

A-S Rollier[1], B Legrand[1], D Collard[2] and L Buchaillot[1]

1 Institut d'Electronique, de Microélectronique et de Nanotechnologie, IEMN, ISEN Department, UMR CNRS 8520, Cité Scientifique, Avenue Poincaré, BP 60069, 59652, Villeneuve d'Ascq, France
2 LIMMS/CNRS-IIS (UMI 2820), Institute of Industrial Science, University of Tokyo, 4-6-1, Komaba, Meguro-ku, Tokyo, 153-8505, Japan

E-mail: anne-sophie.rollier@isen.iemn.univ-lille1.fr and dominique.collard@isen.iemn.univ-lille1.fr

Abstract
This paper deals with parallel-plate electrostatic actuators in liquids. We study the stability conditions of such actuators and show that the pull-in effect can be shifted beyond one-third of the gap, and can even be suppressed. We demonstrate that the insulating layers of the actuator plates, which are originally designed to avoid any current leakages or short-circuits, play a major role in this phenomenon. Experiments are performed on fabricated devices; silicon nitride layers are used to completely encapsulate the actuator plates. The voltages required to close the actuator gap are measured in various liquids and compared to the values obtained by analytical calculations. This study gives guidelines for the design of parallel-plate actuators featuring in liquids either a binary-state operation when the pull-in effect occurs, or a continuous displacement within the full gap.

1. Introduction

Air or vacuum operation of electrostatic actuators is well controlled as well as their technological fabrication. Some systems have been commercialized, such as the digital micromirror device (DMD) invented in 1987 by Texas Instruments, which is a fast reflective digital light electrostatic switch [1].

However, one of the most ambitious applications would be to make them usable in a liquid environment and thus to consider original biomedical applications such as cellular handling and characterization, DNA manipulation or device motion in liquid environment. Only a few devices have been actuated in liquid solutions, such as electrostatic comb-drives insulated using native silicon dioxide (SiO_2) [2].

A great advantage of electrostatic actuation in a liquid environment comes from the relative dielectric constant of liquid, e.g., 80.1 for deionized water and 21 for isopropyl alcohol [3], which is expected to magnify the produced forces. This is quite interesting for low voltage CMOS compatible applications.

In this paper, we focus on the parallel-plate electrostatic actuators that exhibit the well-known pull-in effect in air, which limits the stable positioning of the actuator to one-third of the gap prior to collapse. Some authors have extended the stable operating range of such actuators by using a current pulse drive method [4] or adding external series capacitors [5]. In this work, we demonstrate that the travel range of the actuator in liquids is also affected by the plate insulating layers, even leading to the suppression of the pull-in effect.

Test devices are fabricated with standard silicon microtechnologies. Only a few materials are suitable to insulate the actuator structural parts: silicon nitride, silicon dioxide and various types of resists. The resists cannot

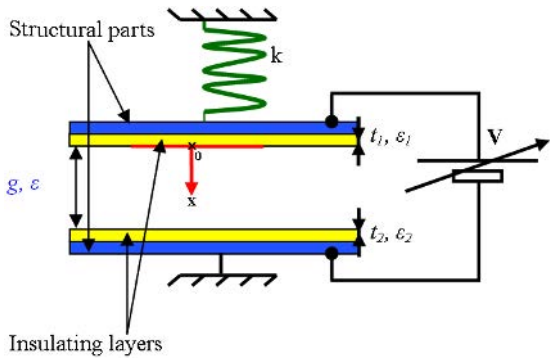

Figure 1. Schematic view of a parallel-plate electrostatic actuator.

be selected because the fabrication of electrostatic actuators requires high temperatures annealing steps. Furthermore, the releasing of the devices is performed by a wet etching of a sacrificial oxide layer. Thus insulating the structural parts with oxide is impossible, except if the oxide growth occurs after the releasing, as in [2]. However, silicon dioxide presents a strong compressive stress so that it is difficult to produce flat devices. Hence, we chose a fabrication process based on a low stress silicon nitride (Si_xN_y) encapsulation of electrostatic actuators.

Since the encapsulation is performed with low stress layers, the structure exhibits no deflection and the topography is very flat. Finally, the breakdown field of Si_xN_y is higher than that of SiO_2 (respectively, 7 MV cm^{-1} against 1.7 MV cm^{-1}, measured in our laboratory) which enables the use of thinner encapsulation thicknesses.

In order to have actuation in liquids and avoid charged bilayer formation and potential screening, an ac drive signal is preferred to the dc polarization of the actuator [2].

The voltages required to close the actuator gap are measured in various liquids and compared to the ones obtained through analytical calculations. This study gives guidelines to design parallel-plate actuators featuring either a binary-state operation when the pull-in effect occurs, or a continuous displacement within the full gap in liquids.

2. Analytical modelling of actuation

The parallel-plate actuator can be typically considered as a capacitor having a fixed electrode while the second electrode is connected to a mechanical spring and is free to move vertically once an electrostatic force is applied; see figure 1. The electrostatic force acts to reduce the gap between the two electrodes. The restoring mechanical force that is exerted by the spring on the mobile electrode is proportional to the spring stiffness and to its deformation [6].

By using the principle of virtual work, the electrostatic force acting on the upper electrode is given by

$$F_{\text{elect}} = \frac{1}{2} \times \frac{\varepsilon_0 \varepsilon \times S \times V^2}{\left[\frac{t_1 \varepsilon}{\varepsilon_1} + \frac{t_2 \varepsilon}{\varepsilon_2} + (g - x)\right]^2} \quad x \in [0, g[\qquad (1)$$

where k is the spring constant, g the gap between the electrodes, V the supply voltage, x the displacement of the mobile part, S the surface of the mobile part, t_1 the thickness of insulating layer 1, ε_1 the relative permittivity of layer 1, t_2 the thickness of insulating layer 2, ε_2 the relative permittivity of layer 2 and ε the permittivity of the medium between the two electrodes.

The equilibrium position of the actuator is reached once the electrostatic and mechanical forces compensate. By using (1),

$$F_{\text{elect}} + F_{\text{mecha}} = 0$$
$$\Leftrightarrow \quad \frac{1}{2} \times \frac{\varepsilon_0 \varepsilon \times S \times V^2}{\left[\frac{t_1 \varepsilon}{\varepsilon_1} + \frac{t_2 \varepsilon}{\varepsilon_2} + (g - x)\right]^2} = k \times x. \qquad (2)$$

Solving equation (2) makes its possible to determine the position x of the actuator according to the voltage V, under the condition that a stable equilibrium solution exists.

As we do not introduce any dynamic and inertial effects in (2), this modelling is applicable, from the mechanical point of view, to quasi-static cases, where mobile plate velocity and acceleration induce no resultant forces. This limits the range of working frequencies to those much lower than the natural resonant frequency of the actuator.

From the electrical point of view, the previous calculation of the electrostatic force in equation (1) is valid for a non-conducting liquid (i.e. without ions). For a conducting fluid, the voltage excitation has to be alternative in order to avoid electrode potential screening, as presented in [2].

Assuming an ac driving voltage

$$V_{\text{ac}} = V_{\text{rms}} \sqrt{2} \cos(\omega t). \qquad (3)$$

The electrostatic force becomes

$$F_{\text{elect-ac}} = \frac{1}{2} \times \frac{\varepsilon_0 \varepsilon \times S \times V_{\text{rms}}^2}{\left[\frac{t_1 \varepsilon}{\varepsilon_1} + \frac{t_2 \varepsilon}{\varepsilon_2} + (g - x)\right]^2} \times [1 + \cos(2\omega t)]. \qquad (4)$$

The induced electrostatic force is then a combination of a static force and of a force at the pulsation 2ω.

In this case, a quasi-static displacement of the actuator is achieved if the actuator mechanical response at pulsation 2ω is negligible compared to the actuator resonance frequency, $f_{\text{resonance}}$, that is to say,

$$2\omega \gg 2\pi \times f_{\text{resonance}}. \qquad (5)$$

Under this assumption (5), the modelling we propose remains valid and can be used in the case of ac driving voltage by simply replacing in equation (2) V by the rms value of the ac voltage V_{rms}.

2.1. Stability study

To determine the range of the stable actuation, the force equilibrium condition in (2) can be rewritten as

$$h(x) = f(V). \qquad (6)$$

With for $x \in [0, g[$:

$$h(x) = \left[t_1 \times \frac{\varepsilon}{\varepsilon_1} + t_2 \times \frac{\varepsilon}{\varepsilon_2} + (g - x)\right]^2 \times x \geqslant 0 \qquad (7)$$

$$f(V) = \frac{1}{2} \times \frac{\varepsilon_0 \varepsilon \times S \times V^2}{k} \geqslant 0. \qquad (8)$$

Solving equation (6) yields the equilibrium position of the actuator mobile part provided that a solution exists.

The stable equilibrium actuation zone is defined by the whole actuator position x in which a stable equilibrium occurs between the electrostatic force and the mechanical force.

Graphically, in figure 2, the function $h(x)$ versus the displacement exhibits a maximum x_1 and a minimum x_2

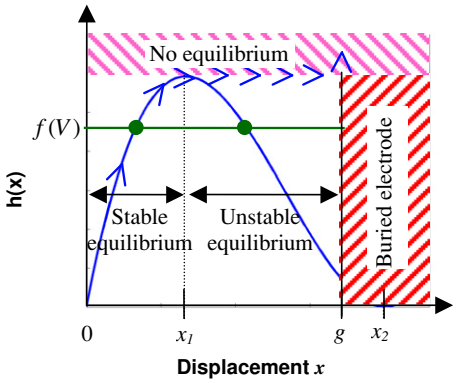

Figure 2. Graphic representation of equation (6). The stable equilibrium position extends from $x = 0$ to $x = \min(g, x_1)$ according to (12). Arrows show the displacement of the actuator when a voltage is applied.

defined by

$$x_1 = \frac{1}{3}\left[\frac{t_1\varepsilon}{\varepsilon_1} + \frac{t_2\varepsilon}{\varepsilon_2} + g\right] \tag{9}$$

$$x_2 = \frac{t_1\varepsilon}{\varepsilon_1} + \frac{t_2\varepsilon}{\varepsilon_2} + g. \tag{10}$$

For a fixed voltage V, two cases must be considered for the resolution of equation (6). If $x \in [0, g[$, $f(V) > h_{\max}(x)$, there is no solution because $F_{\text{elect}} > F_{\text{mecha}}$ and the mobile part collapses onto the buried electrode. There is a new equilibrium in $x = g$ as the reactive force (equivalent to infinite spring stiffness in figure 1) has to be taken into account.

If $x \in [0; g[$, $f(V) < h_{\max}(x)$, as the displacement is limited to $x = g$, and as $g < x_2$ (see equation (10)), there are two equilibrium solutions for equation (6), a stable one before $x = x_1$ and an unstable one after $x = x_1$.

Thus, solving equation (6) yields the extension of the stable actuation zone corresponding to one-third of the initial air-gap. In dielectric liquids, the thickness and permittivity of insulating layers must be taken into account to determine the stable actuation zone.

Then this stable actuation zone ranges from $x = 0$ to $x = \min(g, x_1)$. Since the parallel-plate is voltage controlled, by using (7), (8), (9) and (10), the voltage stable actuation zone can be rewritten as

$$x \in [0, \min(g, x_1)] \quad \Leftrightarrow \quad V \in [0, V(\min(g, x_1))] \tag{11}$$

$$V(g) = \lim_{x \to g} V(x) = \sqrt{\frac{2 \times k \times g \times \left(\frac{t_1\varepsilon}{\varepsilon_1} + \frac{t_2\varepsilon}{\varepsilon_2}\right)^2}{\varepsilon_0\varepsilon \times S}} \tag{12}$$

$$V(x_1) = V_{\text{pull-in}} = \sqrt{\frac{8 \times k \times \left(\frac{t_1\varepsilon}{\varepsilon_1} + \frac{t_2\varepsilon}{\varepsilon_2} + g\right)^3}{27 \times \varepsilon_0\varepsilon \times S}}. \tag{13}$$

Equation (12) corresponds to the voltage required to close the gap g if we are in a stable equilibrium configuration ($g < x_1$). In contrast, if $g > x_1$ the equilibrium is unstable and the *pull-in* effect occurs (see equation (13)).

The stable actuation zone in (8) can be modified to allow controlled motion in the entire gap and to overcome the pull-in effect after initial actuation gap so that pull-in effect does not occurs and the actuator motion is well controlled.

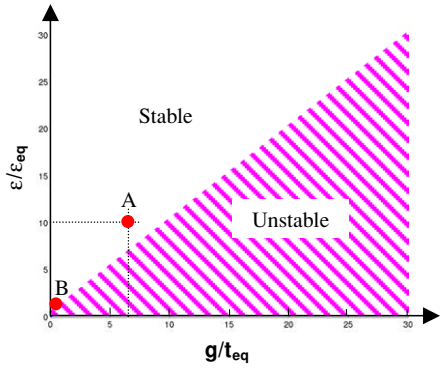

Figure 3. Graphical representation of condition (14). The relative permittivity is plotted versus the normalized thickness. t_{eq} and ε_{eq} are, respectively, the thickness and the permittivity of the insulating layers.

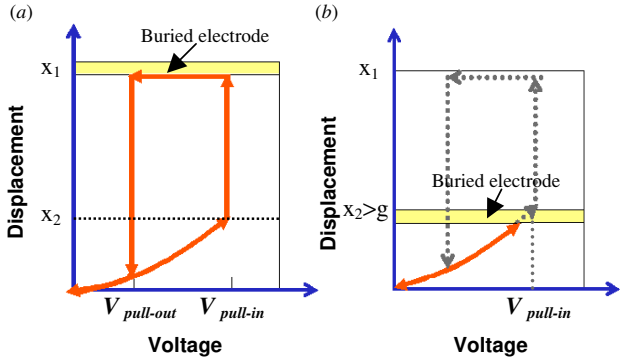

Figure 4. Displacement versus voltage characteristic for electrostatic actuation with pull-in effect (*a*) and without pull-in effect (*b*).

With equation (9), we can obtain stable actuation within the whole gap, if

$$x_1 > g \quad \Leftrightarrow \quad \left[\frac{t_1}{\varepsilon_1} + \frac{t_2}{\varepsilon_2}\right] > \frac{2}{\varepsilon} \times g. \tag{14}$$

If the condition (14) is not observed, then the equilibrium becomes unstable and the moving part collapses; it is the pull-in effect (figure 2).

Indeed, if by construction, the previous condition (14) is respected, then the displacement of the moving part can be controlled within the entire gap.

Figure 3 represents the stability study with respect to the parameters of equation (14). To simplify the representation, the thickness and the permittivity of the two insulating layers are chosen to be equal; thus $t_1 = t_2 = t_{\text{eq}}$ and $\varepsilon_1 = \varepsilon_2 = \varepsilon_{\text{eq}}$.

2.2. *Motion–voltage characteristic*

Solving equation (6) yields the x position of the actuator according to the applied voltage V.

Voltage–displacement characteristic of the actuator is schematically shown in figure 4(*a*) when the condition given in equation (14) is not respected. For a voltage lower than the pull-in voltage, $V_{\text{pull-in}}$, the actuator motion can be controlled until the x_2 position. At $V = V_{\text{pull-in}}$, the upper electrode collapses on the lower one. To release the contact, the voltage

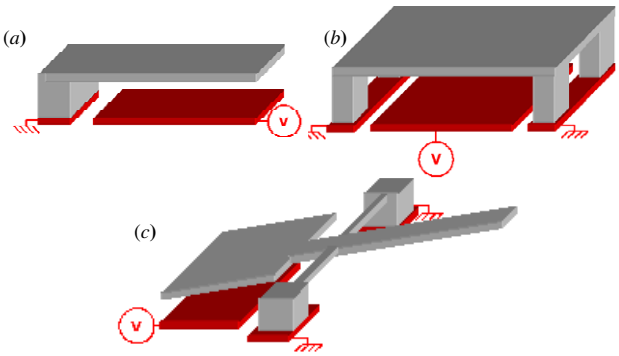

Figure 5. Schematic view of (*a*) a parallel-plate actuator; (*b*) the membrane clamped in its 4 corners and (*c*) the torsional actuator.

has to be reduced until the $V_{\text{pull-out}}$ value, which is the second threshold voltage of this hysteresis cycle. Then the actuator recovers a position in the stable actuation zone.

The *pull-out* voltage depends on the quality of the contact between the mobile part and the buried electrode. In fact, an intimate gap is achieved between the two layers depending on surface roughness, and interactive forces such as Van der Waals. All of these added parameters have to be taken into account to determine the expression of $V_{\text{pull-out}}$ [7].

Figure 4(*b*) represents the case where the condition (14) is fulfilled, and the pull-in effect does not occur. Consequently, the motion of the mobile part can be controlled in the entire gap and there is no hysteresis cycle.

For example, a parallel-plate actuator with $g = 2$ μm and 300 nm thick of Si_xN_y insulating layers ($\varepsilon_{\text{eq}} = 8$) does not exhibit the pull-in effect in water ($\varepsilon = 80.1$). In fact, $V_{\text{pull-in}}$ occurs for a 2.6 μm displacement (see equation (13)) which exceeds the physical gap g (see point A in figure 3).

Whereas, according to point B in figure 3, 24 μm of low stress silicon nitride would have been required in order to actuate the same parallel-plate actuator in air under stable equilibrium condition, which is unrealistic.

Consequently, we chose to encapsulate the structural part of the actuator with 300 nm of Si_xN_y in order to control the motion in the entire gap during actuation in water.

3. Fabrication process

Three types of parallel-plate actuators have been fabricated using the same technological process: a simple parallel-plate device, a torsional actuator with a square electrostatic plate for actuation, two torsional beams and a lever to increase the deflection, and finally a membrane clamped in its four corners; see figure 5.

Starting from a silicon wafer, a 350 nm dry oxidation is performed and a 100 nm Si_xN_y (the exact stoichiometry has been optimized to reduce residual tensile stress) layer is deposited at 800 °C to insulate the substrate; then, a 350 nm n-doped polycrystalline silicon layer is deposited by low pressure chemical vapour deposition (LPCVD), transferred by photolithography and SF_6 reactive ion etching (RIE) to pattern buried electrodes. To insulate the electrodes during actuation, a 300 nm Si_xN_y layer is used; see figure 6(*a*).

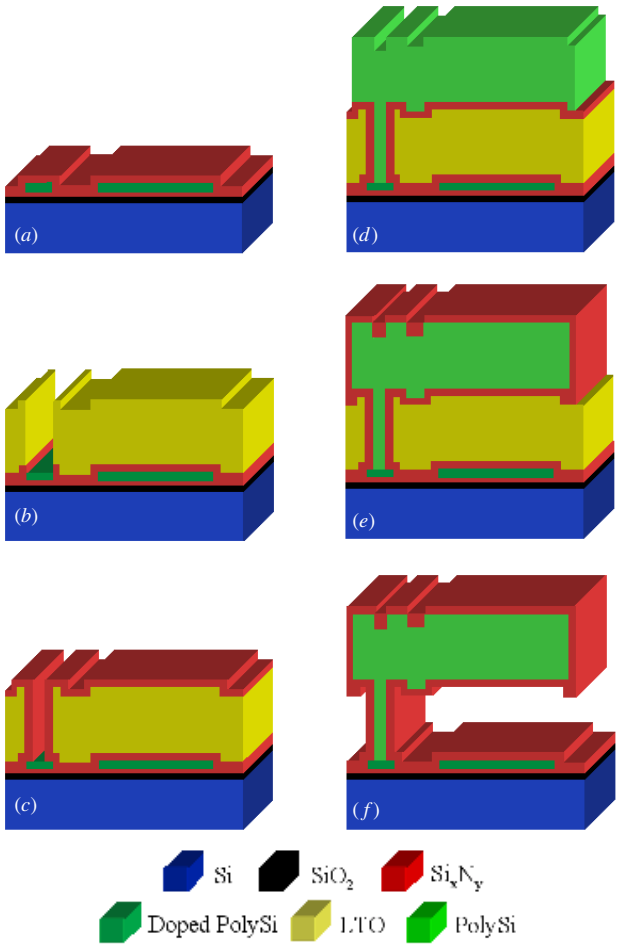

Figure 6. Process flow: (*a*) buried electrodes patterning; (*b*) deposition and etch of the sacrificial layer; (*c*) first level of nitride encapsulation; (*d*) deposition of the structural layer; (*e*) second level of nitride encapsulation; (*f*) releasing in a HF solution.

A 2 μm sacrificial layer of low temperature oxide (LTO) is deposited by LPCVD and anisotropically etched in a CF_4 and CHF_3 plasma; see figure 6(*b*).

Since actuators are operated in a liquid environment, to prevent any short-circuits and electrical leakages through the liquid medium, an encapsulation with Si_xN_y is achieved.

As the breakdown field of Si_xN_y deposited in our laboratory is 7 MV cm^{-1}, the 300 nm thick Si_xN_y layer is able to withstand a breakdown voltage of 200 V.

The first level of encapsulation is made of a 300 nm thick Si_xN_y layer anisotropically etched in order to open the electric contacts; figure 6(*c*). The structural material is a 2 μm n-doped polycrystalline silicon, which is anisotropically etched by SF_6 RIE; see figure 6(*d*). The second 300 nm silicon nitride for the front side insulation is deposited and patterned resulting in the complete encapsulation of the device; see figure 6(*e*).

In order to relax the mechanical stress in the stacked layers, a thermal annealing step is performed at 1100 °C during 3 h. The last step consists in the release of the structure in a hydrofluoric (HF) aqueous solution; see figure 6(*f*).

A parallel-plate actuator is shown in the scanning electron microscopy (SEM) picture in figure 7(*a*); the inset (figure 7(*b*)) shows a zoom of the step covering of the encapsulated layer

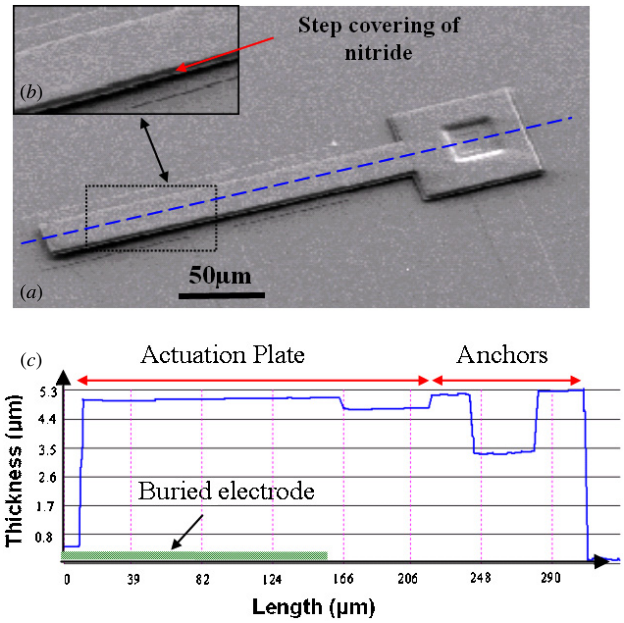

Figure 7. (*a*) SEM image of a parallel-plate actuator. (*b*) Close view of the nitride step covering. (*c*) Profile topography corresponding to dashed line in figure 4(*a*).

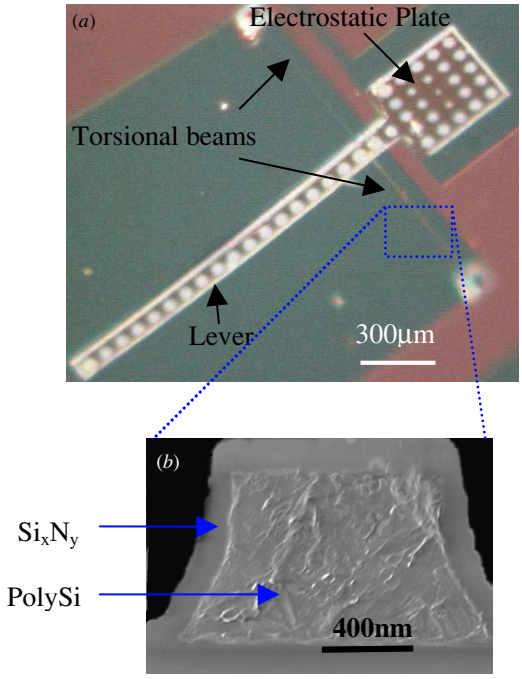

Figure 8. (*a*) Optical microscope image of a torsional actuator. (*b*) SEM image of cross section of the parallel-plate actuator encapsulated with Si_xN_y corresponding to the tire line in figure 5(*a*).

of Si_xN_y. In order to validate the fabrication process, an interferometrical profile image has been performed along the cantilever (figure 7(*c*)). We can see that the profile topography is flat; thus no deflection appears which means that there is no notable stress gradient in the structure.

In order to precisely see the Si_xN_y encapsulation, a cross-section is made on a very small structure, a 2 μm width and 2 μm thick beam (figure 8(*a*)). A SEM image of the cross section of the beam encapsulated with 300 nm of low stress

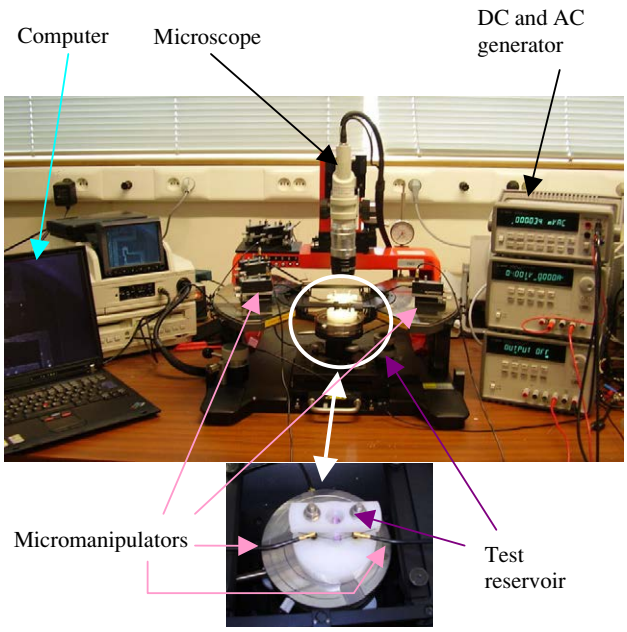

Figure 9. Experimental set-up. A probe station is used to keep the contact and see the motion of the actuator. A test box enables the introduction and the removal of liquid, the electrical contact is taken out of the box.

silicon nitride is presented in figure 8(*b*); we clearly see the 2 μm polycrystalline silicon surrounded by a 300 nm Si_xN_y layer.

4. Experimental characterization

Experiments have been performed in different solutions with various permittivity and conductivity such as air, pure deionized water, isopropyl alcohol (IPA) and tap water. The three types of actuators have been tested, parallel-plate, torsional actuator and membrane. The devices have been tested using the experimental set-up shown in figure 9. A liquid reservoir is used to introduce the fluid into the sample, whilst keeping electrical contacts in a dry environment. The contacts are made by using two micromanipulators. A probe station enables the displacement visualization by way of an optical microscope. The dc and the ac polarization are generated by a waveform generator, connected to the device contacts and in parallel with an oscilloscope to monitor the voltage.

4.1. Electrode potential screening

As actuation occurs in dielectric liquid environment, during actuation ions accumulate in a electrical double layer (EDL) at the electrode interface; thus there is a phenomenon of potential screening [9]. Then, as deionized water presents an ionic strength around 10^{-7} mol l^{-1}, potential screening is also possible and has been estimated from the Gouy–Chapman model [10] by [9]. To avoid EDL, actuation must be driven by ac signals. The frequency of the signal to be employed depends on the dimensions of the structure (the dielectric layer thickness t_{eq} and the gap g), and the liquid conductivity. Sounart *et al* [9] give us a reference chart for determining the actuation frequency. For deionized water, the minimum applied frequency must be 13 kHz. In the case of IPA, the

Table 1. Minimum driving frequency in dielectric liquid.

Liquid	Conductivity[b]	Frequency[a]
Isopropyl alcohol	0.09 μS cm^{-1}	17 kHz
Deionized water	0.07 μS cm^{-1}	13 kHz
Tap water	5 μS cm^{-1}	1 MHz

[a] Value from [9] with a 300 nm thickness of dielectric layer and a 2 μm gap between the mobile part and the buried electrode.
[b] Value from [3].

Table 2. Parameters of the cantilever type actuator.

Parameter	Value
Actuator length L	$L = 250$ μm
Actuator width w	$w = 30$ μm
Actuator thickness t	$t = 2$ μm
Actuator mobile part surface S	$S = 6000$ μm^2
Actuator effective stiffness k	$k = 0.8$ N m^{-1}
Gap between the actuator and the electrode g	$g = 2$ μm
Insulating layer 1 thickness t_1	$t_1 = 300$ nm
Insulating layer 1 relative permittivity[a] ε_1	$\varepsilon_1 = 8$
Insulating layer 2 thickness t_2	$t_2 = 300$ nm
Insulating layer 2 relative permittivity[a] ε_2	$\varepsilon_2 = 8$
Dielectric permittivity ε_0	$\varepsilon_0 = 8.85 \times 10^{-12}$ F m^{-1}

[a] Values from Si_xN_y [8].

driving frequency has to be higher than 17 kHz; in the case of tap water, the critical frequency is 1 MHz (table 1).

Thus, the devices have been tested at 1 MHz, in the different fluids, in order to avoid charged bilayers and potential screening, which is likely to decrease the electrostatic force and thus lose the actuation [11, 12].

4.2. Parallel-plate actuator

A parallel-plate actuator with the dimensions given in table 2 has been fabricated to test the out-of-plane displacement; the optical image in figure 10 was taken during actuation in tap water. Figure 10(*a*) corresponds to the upper position at $V = 0$ V. In figure 10(*b*) the 2 μm gap between the mobile part and the buried electrode is closed.

The structure has been firstly tested in air with and without the Si_xN_y encapsulation. Since condition of equation (14) is not respected, the pull-in effect occurs, respectively, at 7 V and 8 V either without or with the nitride encapsulation (table 3). We can see that the two 300 nm thick dielectric layers induce an increasing in the actuation voltages by 15%.

If we raise the relative permittivity of the medium by actuating the parallel-plate in IPA, the condition (14) is not respected any longer and the pull-in effect appears at 4 V (table 3). The actuation voltage is reduced by 50% compared to the one in air.

The last two tests occur in deionized and in tap water; thus the condition (14) is satisfied and the motion of the mobile part is controlled within the entire gap, the voltage to close the 2 μm gap is around 6 V (table 3).

These preliminary tests show that the electrostatic actuation principle can be applied to a large range of fluids with various permittivity and conductivity.

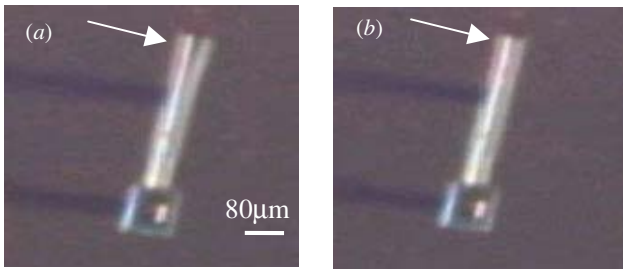

Figure 10. (*a*) Optical image during actuation in water when the gap is open. (*b*) Optical image during actuation in water when the 2 μm gap is closed. White arrows show actuation location.

Table 4. Parameters of the torsional actuator tested.

Parameter	Value
Actuator length L	$L = 300$ μm
Actuator width w	$w = 300$ μm
Actuator thickness t	$t = 2$ μm
Actuator mobile part surface S	$S = L \times w = 0.09$ mm^2
Actuator effective stiffness k	$k = 3.26 \times 10^{-9}$ N m rad^{-1}
Torsional beam length L_t	$L_t = 490$ μm
Torsional beam width w_t	$w_t = 5$ μm
Lever beam length L_l	$L_l = 1100$ μm
Lever beam width w_l	$w_l = 90$ μm
Gap between the actuator and the electrode g	$g = 2$ μm
Insulating layer 1 thickness t_1	$t_1 = 300$ nm
Insulating layer 1 relative permittivity[a] ε_1	$\varepsilon_1 = 8$
Insulating layer 2 thickness t_2	$t_2 = 300$ nm
Insulating layer 2 relative permittivity[a] ε_2	$\varepsilon_2 = 8$
Dielectric permittivity ε_0	$\varepsilon_0 = 8.85 \times 10^{-12}$ F m^{-1}

[a] Values from Si_xN_y [3].

4.3. Other structures

To study electrostatic actuation in liquid medium, the other types of actuators have been tested with the same experimental set-up than in figure 9.

Table 3. Theoretical and experimental voltage for the parallel-plate tested in different liquid medium with the dimension in table 1.

Actuation	Relative permittivity[a]	Theoretical voltage to to close the 2 μm gap (V)	Experimental voltage to close the 2 μm gap (V)	Difference (%)
Air (without Si_xN_y)	1	$V_{\text{pull-in}} = 7.31$	$V_{\text{pull-in}} = 7$	4
Air (with Si_xN_y)	1	$V_{\text{pull-in}} = 7.73$	$V_{\text{pull-in}} = 8$	3.4
Isopropyl alcohol (1 MHz)	21.3	$V_{\text{pull-in}} = 3.78$	$V_{\text{pull-in}} = 4$	5.8
Deionised water (1 MHz)	80.1	$V_{(2\ \mu\text{m})} = 6.37$	$V_{(2\ \mu\text{m})} = 6$	5.8
Tap water (1 MHz)	80.1	$V_{(2\ \mu\text{m})} = 6.37$	$V_{(2\ \mu\text{m})} = 6$	5.8

[a] Values from Si_xN_y [3].

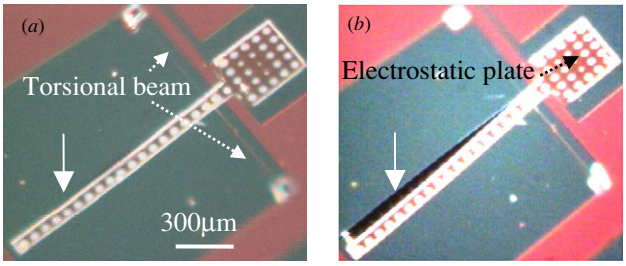

Figure 11. (*a*) Optical image of a torsional actuator during actuation in water when the gap is open. (*b*) Optical image of a torsional actuator during actuation when the 2 μm gap is closed. White arrows show actuation location.

Table 5. Parameters of the membrane tested.

Parameter	Value
Actuator length L	$L = 378$ μm
Actuator width w	$w = 243$ μm
Actuator thickness t	$t = 2$ μm
Actuator mobile part surface S	$S = L \times w = 91854$ μm^2
Gap between the actuator and the electrode g	$g = 2$ μm
Insulating layer 1 thickness t_1	$t_1 = 300$ nm
Insulating layer 1 relative permittivity[a] ε_1	$\varepsilon_1 = 8$
Insulating layer 2 thickness t_2	$t_2 = 300$ nm
Insulating layer 2 relative permittivity[a] ε_2	$\varepsilon_2 = 8$
Dielectric permittivity ε_0	$\varepsilon_0 = 8.85 \times 10^{-12}$ F m^{-1}

[a] Values from Si_xN_y [3].

An interesting type of actuation in liquid environment is the torsional electrostatic actuation [13] which could be used to make a micro-gripper. To highlight this principle, parallel-plate structures are maintained by fixed beams; thus during actuation, these beams are subjected to mechanical moments of torsion [14, 15]. The picture in figure 11 shows a torsional actuator with a square electrostatic plate for actuation and two torsional beams; the deflection is observed on a lever beam, dimensioned in table 4.

This device has been tested in air, in tap water and in IPA (table 6). The $V_{\text{pull-in}}$ voltages are lower than the ones in the previous design, because of the higher surface of the actuation (see equation (13)).

As actuation occurs in a liquid environment, actuation involves fluid displacement. To test the robustness of the

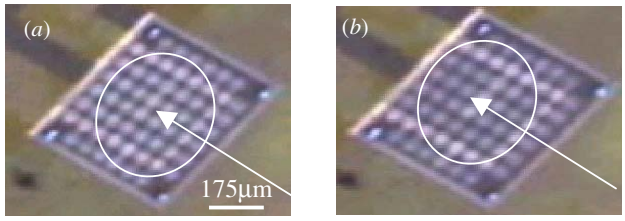

Figure 12. (*a*) Optical image of a membrane during actuation in water when the gap is open. (*b*) Optical image of a membrane during actuation when the 2 μm gap is closed. White arrows show actuation location.

structures, a membrane clamped in its four corners was fabricated with a 300 nm Si_xN_y encapsulation. The dimensions of the membrane are given in table 5. Figure 12 presents a microscope image of the membrane. The membrane has been actuated in air, in tap water and in IPA; the results are presented in table 6. We note a good agreement between experimental and modelled values. This type of design presents a strong effective stiffness, which explains the high values of the pull-in voltages (see equation (13)).

In figures 11 and 12, some holes were bored in the structural part to allow a better release of the membrane and the torsional actuator. Indeed, this release is carried out in liquid medium and these holes support the flow of HF.

5. Conclusion

In this paper, we have presented a novel optimized fabrication technique of parallel-plate actuators with a complete Si_xN_y encapsulation, allowing electrostatic actuation in a liquid environment. Analytical calculations show that the pull-in effect can be shifted far beyond one-third of the gap and even suppressed. The thicknesses and dielectric constants of the insulating layers play a major role in this phenomenon. Experiments have been performed on fabricated devices and actuation has been successfully observed on cantilevers, torsional actuators and membranes. The voltages required to close the actuators gap have been measured in IPA, DI water and tap water. They are in good agreement with the theoretical values. Further investigations will concern the dynamic behaviour of the actuators in liquids, which is strongly affected by a much higher damping coefficient in liquids than in air [16–18].

Table 6. Simulated and experimental voltage for torsional actuator and membrane in different liquid mediums with the dimension in table 3.

Type of structure	Actuation	Air (with Si_xN_y)	Isopropyl alcohol (1 MHz)	Water (1 MHz)
	Relative permittivity[e]	1	21.3	80.1
Torsional actuator[a]	Theoretical voltage[b]	$V_{\text{pull-in}} = 0.25$ V	$V_{\text{pull-in}} = 0.12$ V	$V_{(2\ \mu\text{m})} = 0.19$ V
	Experimental voltage[c]	$V_{\text{pull-in}} = 0.3$ V	$V_{\text{pull-in}} = 0.16$ V	$V_{(2\ \mu\text{m})} = 0.23$ V
Membrane[d]	Simulated voltage[f]	$V_{\text{pull-in}} = 44.68$ V	$V_{\text{pull-in}} = 16.37$ V	$V_{(2\ \mu\text{m})} = 33.4$ V
	Experimental voltage[c]	$V_{\text{pull-in}} = 45$ V	$V_{\text{pull-in}} = 15.9$ V	$V_{(2\ \mu\text{m})} = 33.9$ V

[a] Dimensions in table 3.
[b] Theoretical voltage to close the 2 μm gap.
[c] Experimental voltage to close the 2 μm gap.
[d] Dimensions in table 4.
[e] Values from Si_xN_y [3].
[f] Simulated with CoventorWare™ software.

Acknowledgment

The authors would like to thank the valuable work of the IEMN technical staff, and the 'Délégation Générale pour l'Armement' for the financial support of A-S Rollier.

References

[1] Gove R J 2004 DMD Display systems: the impact of an all-digital display *Int. Symp. Society for Information Display*

[2] Sounart T L and Michalske T A 2003 Electrostatic actuation without electrolysis in microfluidic MEMS *Transducers'03* pp 615–8

[3] Janz G J and Tomkins R P T 1972 *Nonaqueous Electrolytes Handbook: Volume 1* (New York: Academic)

[4] Castaner L, Pons J, Nadal-Guardia R and Rodriguez A 2001 Analysis of the extended operation range of electrostatic actuators by current-pulse drive *Sensors Actuators* A **90** 181–90

[5] Chan E K and Dutton R W 2000 Electrostatic micromechanical actuator with extended range of travel *J. Microelectromech. Syst.* **9** 321–8

[6] Senturia S D 2001 *Microsystem Design* (Dordrecht, MA: Kluwer)

[7] Rebeiz G M (ed) 2003 *RF MEMS: Theory, Design, and Technology* (New York: Wiley)

[8] Sze S M (ed) 1981 *Physics of Semiconductor Devices* 2nd edn (New York: Wiley)

[9] Sounart T L, Michalske T A and Zavadil K R 2005 Frequency-dependent electrostatic actuation in microfluidic MEMS *J. Microelectromech. Syst.* **14** 125–33

[10] Hunter R J 1981 *Zeta Potential in Colloid Science: Principles and Applications* (London: Academic)

[11] Pomes V, Fernandez A, Costarramone N, Grano B and Houi D 1999 Fluorine migration in a soil bed submitted to an electric field: influence of electric potential on fluorine removal *Colloids Surf.* A 481–90

[12] Ho C-M and Tai Y-C 1998 Micro-electro-mechanical-systems (MEMS) and fluid flows *Annu. Rev. Fluid Mech.* **30** 579–612

[13] Toshiyoshi H and Fujita H 1996 Electrostatic micro torsion mirrors for an optical switch matrix *J. Microelectromech. Syst.* **5** 231–7

[14] Degani O, Socher E, Lipson A, Lejtner T, Setter D J, Kaldor S and Nemirovsky Y 1998 Pull-in study of an electrostatic torsion microactuator *J. Microelectromech. Syst.* **7** 373–9

[15] Satter R, Plötz F and Wachutta G 2001 Macromodeling of an electrostatic torsional actuator *Transducers'01 (Munich)*

[16] Lin G, Palmer R E, Pister K S J and Roos K P 2001 Miniature heart cell force transducer system implemented in MEMS technology *IEEE Trans. Biomed. Eng.* **48** 996–1006

[17] Maali A, Hurth C, Boisgard R, Jai C, Cohen-Bouhacina T and Aimé J-P 2005 Hydrodynamics of oscillating atomic force microscopy cantilevers in viscous fluids *J. Appl. Phys.* **97** 074907

[18] Bouhacina T, Michel D, Aimé J-P and Gauthier S 1997 Oscillation of the cantilever in atomic force microscopy: Probing the sample response at the microsecond scale *J. Appl. Phys.* **82** 3652–60